Available online at www.sciencedirect.com
ScienceDirect
Journal of the European Ceramic Society 30 (2010) 591–598
www.elsevier.com/locate/jeurceramsoc

Polymer-assisted precipitation of ZnO nanoparticles with narrow particle size distribution

Anne Aimable [a,*], Maria Teresa Buscaglia [b], Vincenzo Buscaglia [b], Paul Bowen [a]

[a] *Powder Technology Laboratory (LTP), Materials Institute, Swiss Federal Institute of Technology, Ecole Polytechnique Fédérale de Lausanne (EPFL), 1015 Lausanne, Switzerland*

[b] *Institute for Energetics and Interphases, Department of Genoa, National Research Council, 16149 Genoa, Italy*

Available online 19 July 2009

Abstract

Zinc oxide nanoparticles were produced by aqueous precipitation in mild hydrothermal conditions (90 °C). Well crystallized regular roundish particles were obtained, with a very narrow size distribution. The influence of soft templates (organic species) to control size and size distribution in the final product was investigated. No effect was observed with polyvinylpyrrolidone (PVP M_w 8000 and 40,000), (D−)fructose and hydroxypropylmethylcellulose (HPMC). A significant decrease of the particle size towards 100 nm, while conserving a very narrow size distribution was observed for poly(acrylic acid) (PAA M_w 2000), Dispex A40 (commercial PAA from CIBA M_w ∼10,000), and sodium dodecylsulfate (SDS). The influence of the pH was also investigated with PAA. By increasing the pH from slightly acidic to basic conditions, the morphology was spectacularly modified from roundish nanoparticles to micronic branched flower-like particles, with an elongated primary crystal morphology.

Keywords: Powder chemical preparation; Grain size; Particle size distribution; ZnO

1. Introduction

Zinc oxide is a material that exhibits semiconducting, piezoelectric, and pyroelectric properties. Major industrial applications include electronic devices such as gas sensors or varistors.[1] Optical properties are also widely exploited, as a dye (zinc white), or UV-light emitter. More recently, Al-doped ZnO has attracted scientists' interest for applications as a transparent and conducting coating for solar cells. Thus by tuning the formulation (dopant addition), it is possible to enlarge the field of its application.

The development of zinc oxide in new attractive markets imposes severe constraints where a high-value material at a competitive price is a key factor. Most applications need ceramics with a high density achieved through a good control of the material at all processing stages from synthesis, forming and sintering.

Numerous routes are available for ZnO synthesis for example, physical routes, such as vapour phase methods[2,3] and spray pyrolysis.[4] Recently submicron ZnO crystals have been obtained with an ultrasonic spray pyrolysis method[5]: The main drawback is the high temperatures applied, from 200 to 600 °C, which makes this process costly. Wet chemistry, including precipitation,[6–9] hydrothermal[2,10–12] and solvothermal[13] synthesis, microemulsions,[14] and sol–gel processes[15,16] have succeeded in the controlled synthesis of numerous shapes, sizes and morphologies, at low temperature. Among these routes, the low cost and simplicity of aqueous precipitation make this approach the most attractive, for possible commercial development. Once the conditions of the synthesis have been determined in simple batch reactors, the production of such powders can be transferred to innovative reactors such as the segmented flow tubular reactor (SFTR),[17] a continuous process which allows an easy up-scaling from the laboratory experiments to the production scale without loss of product quality.

A better control of the precipitate can often be achieved with respect to its size, shape, and chemical composition, with the use of polymeric additives.[18,19] By changing the charge at the surface of the particles, or by adsorbing onto specific crystal planes, modification of the crystal growth can be induced.[20] Polymer-assisted ZnO synthesis has succeeded in tuning particle size and morphology, leading to various shapes such as hexagonal

* Corresponding author. Tel.: +41 21 693 51 09; fax: +41 21 693 30 89.
E-mail address: anne.aimable@epfl.ch (A. Aimable).

0955-2219/$ – see front matter © 2009 Elsevier Ltd. All rights reserved.
doi:10.1016/j.jeurceramsoc.2009.06.010

Table 1
Experimental conditions for ZnO powders synthesized in a mini-batch reactor.

Sample	$[Zn^{2+}]$ reaction solution [mol L^{-1}]	$[HO^-]$ reaction solution [mol L^{-1}]	Additive 0.05 wt.% in $[HO^-]$ reaction solution	pH
$ZnO_{[0.11]}$	0.10	0.11	–	5.6
$ZnO_{[SDS]}$	0.10	0.11	SDS	5.6
$ZnO_{[fru]}$	0.10	0.11	Fructose	5.6
$ZnO_{[HPMC]}$	0.10	0.11	HPMC	5.6
$ZnO_{[PVP8000]}$	0.10	0.11	PVP 8000	5.6
$ZnO_{[PVP40,000]}$	0.10	0.11	PVP 40,000	5.6
$ZnO_{[Disp]}$	0.10	0.11	Dispex A40	5.6
$ZnO_{[PAA]}$	0.10	0.11	PAA 2000	5.6
$ZnO_{[PAA-0.22]}$	0.10	0.22	PAA 2000	11.2
$ZnO_{[PAA-1.5]}$	0.10	1.50	PAA 2000	12.5

Plates,[21] flower-like particles,[7,22] or nanorods.[6,8,23,24] As far as we know only a few papers[2,9,10] present the synthesis of regular nanoparticles, although they should be the best candidate for forming dense nanostructured ceramics.

Our objective is the synthesis of ZnO nanoparticles (<100 nm), with a homogeneous morphology and a narrow particle size distribution. The synthesis has been conducted in a small volume batch reactor (40 mL), designed to allow a fast and efficient mixing of the aqueous reaction solutions. The influence of additives on the final product was investigated, as well as the influence of pH related to structural and thermodynamic considerations.

2. Materials and methods

ZnO was produced by mixing zinc nitrate and sodium hydroxide aqueous solutions (Eq. (1))

$$Zn^{2+}{}_{(aq)} + 2HO^{-}{}_{(aq)} \rightarrow ZnO_{(s)} + H_2O \quad (1)$$

The Zn^{2+} reactant solution was prepared by dissolving $Zn(NO_3)_2{\cdot}6H_2O$ in ultra pure water. The NaOH solution was prepared by diluting a titrated solution NaOH 1 M or solid NaOH depending on the concentration needed. Both solutions were filtered at 0.2 μm before use. The various additives studied were introduced by dissolving 0.05 wt.% in the NaOH reaction solution. Poly(acrylic acid) (PAA) with two different molecular weights was chosen as an anionic polyelectrolyte: PAA $M_w = 2000$, and Dispex A40 (commercial PAA from CIBA $M_w \sim 10{,}000$). Polyvinylpyrrolidone (PVP) with two molecular weights ($M_w = 8000$ and $M_w = 40{,}000$) was chosen as non-ionic polymer. Sodium dodecylsulfate (SDS) was tested as anionic surfactant. (D−)fructose and hydroxypropylmethylcellulose (HPMC) were chosen among the carbohydrates category of non-ionic polymers. The pH of the reaction was changed by addition of NaOH. Precipitation reactions were carried out in a 40 mL fed-batch reactor, hereafter called "mini-batch reactor". Good mixing between the two reactants was achieved by using a Y mixer. The injection of the reactant took 4 s, and was achieved by an automatic injection with 20 mL syringes (Hamilton). The effective mixing time was evaluated to be 50–100 ms.[19] The reactor was heated at 90 °C by an external circulation of hot water (95 °C). After mixing the reaction mixture was aged during 30 min. Then the reactor was placed in a bath of cold water for cooling. The reaction mixture was then washed with ultra pure water, before being filtered and dried for 24 h at room temperature under a low vacuum. The experimental conditions are summarized in Table 1.

The phase identification of the precipitates was made with powder X-ray diffraction (XRD, Philips X'Pert diffractometer, Cu K_α radiation). XRD peak broadening was used to determine the size of the primary crystallite using the Scherrer equation (Eq. (2)). The instrumental broadening was determined using alumina with a large crystal size (>1 μm)

$$d_{XRD} = \frac{K\,\lambda_X}{\beta_{Xp}\cos(\theta)} \quad (2)$$

where K is equal to 0.9, λ_X is the X-ray wavelength, β_{Xp} is the integral breadth of the material, calculated using $\beta_{Xp} = \sqrt{(\beta^2 - \beta^2_{alumina})}$, and β the integral breadth is the ratio of the area and the height of the diffraction peak.

The powder morphologies were analyzed by scanning electron microscopy (SEM, Philips XL 30 FEG microscope). The SEM samples were prepared by dispersing the powder in ethanol. One drop of the suspension was then deposited on an aluminum support and dried in air. Brunauer–Emmett–Teller (BET) specific surface areas S_{BET} ($m^2\,g^{-1}$) were estimated from N_2 adsorption isotherms (Micromeritics Gemini 2375). The size of the primary particles, d_{BET} (nm), were calculated by assuming spherical monodisperse particles (Eq. (3)), with ρ the density of the material ($\rho = 5.6\ g\,cm^{-3}$)

$$d_{BET} = \frac{6000}{S_{BET}\rho} \quad (3)$$

Before BET measurements the samples were dried at 200 °C in flowing nitrogen for 1 h.

The particle size distribution was collected using a centrifugal method (CPS, Disc Centrifuge Model DC 24,000). For this measurement, powders were suspended in a solution of PAA 0.1% (pH ~10, concentration 0.01 wt.%). Thermogravimetric curves (TGA, Mettler TGA/DSC/TMA analyzer) were collected from room temperature to 800 °C under flowing air at a heating rate of 10 °C/min.

Table 2
Results of S_{BET}, d_{BET} and d_{XRD} of ZnO powders obtained in different conditions, and on samples $ZnO_{[SDS]}$, $ZnO_{[Disp]}$ and $ZnO_{[PAA]}$ after a heat treatment of 10 min at 500 °C.

Sample	S_{BET} [$m^2 g^{-1}$]	d_{BET} [nm]	d_{XRD} along [1 0 0] [nm]	d_{XRD} along [0 0 2] [nm]	After a heat treatment of 10 min at 500 °C			
					S_{BET} [$m^2 g^{-1}$]	d_{BET} [nm]	d_{XRD} along [1 0 0] [nm]	d_{XRD} along [0 0 2] [nm]
$ZnO_{[0.11]}$	9.5	112	27	37				
$ZnO_{[SDS]}$	35.5	30	27	29	26.6	40	28	28
$ZnO_{[fru]}$	7.7	140	28	39				
$ZnO_{[HPMC]}$	9.8	109	27	39				
$ZnO_{[PVP8000]}$	6.4	166	27	35				
$ZnO_{[PVP40,000]}$	7.1	151	28	37				
$ZnO_{[Disp]}$	40.3	27	25	29	12.4	86	28	28
$ZnO_{[PAA]}$	75.0	14	24	31	14.7	73	28	30
$ZnO_{[PAA-1.5]}$	2.9	365	41	41				

3. Results

3.1. X-ray diffraction (XRD)

XRD patterns of all the samples were all similar to the XRD pattern of $ZnO_{[0.11]}$ obtained at low pH without an additive and presented Fig. 1. In all cases a crystalline material was produced, which matched the ZnO pattern of wurtzite (ICDD 075-0576). Crystallite sizes were calculated using the [1 0 0] reflection and were in the same range, between 24 and 28 nm (Table 2). An exception was $ZnO_{[PAA-1.5]}$, obtained in basic conditions which showed a value of 41 nm. The crystallite size deduced from the broadening of the [0 0 2] reflection were higher than those calculated from the [1 0 0] reflection for all the samples, with a ratio varying from 1.0 to 1.4. This indicates a small elongation of the crystallites in the direction of the *c*-axis, often seen in other studies, and attributed to the hexagonal structure of the wurtzite.[9]

3.2. Specific surface area (BET)

The S_{BET} and the corresponding calculated primary particle size (d_{BET}) are presented in Table 2. The material obtained at low pH without an additive ($ZnO_{[0.11]}$) presented an S_{BET} of 9.5 $m^2 g^{-1}$, corresponding to a d_{BET} of 112 nm. The additives had different effects on the S_{BET}. Fructose, PVP 8000 and PVP 40,000 led to a smaller S_{BET}, whereas HPMC induced almost no change. The addition of PAA 2000, Dispex A40 and SDS led to a significant increase of S_{BET}, to 75.0, 40.3, and 35.5 $m^2 g^{-1}$, respectively. A heat treatment of 10 min at 500 °C was used to burn out the adsorbed polymer. This treatment induced a small increase of the crystallite size of ZnO measured along [1 0 0] (by 1–4 nm). The sample obtained in basic conditions ($ZnO_{[PAA-1.5]}$) had a low S_{BET} of 2.9 $m^2 g^{-1}$, corresponding to a d_{BET} of 365 nm.

3.3. Thermogravimetric analysis (TGA)

The TG curve for sample $ZnO_{[0.11]}$ synthesized at pH = 5.6 without an additive is presented in Fig. 2. The first weight loss (between 30 and 200 °C) was attributed to the removal of physically adsorbed water. The second weight loss (between 200 and 600 °C) was attributed to the decomposition of chemically bound hydroxyl groups. The total weight loss was small with a value of 2.9%. In the case of samples synthesized with additives, the removal of the organic compounds that were adsorbed at the surface occurs in between 200 and 600 °C and gave a significant increase of the total weight loss (Table 3). The weight losses measured at 500 and 800 °C are very similar indicating that after 10 min at 500 °C, all the adsorbed polymer should be removed.

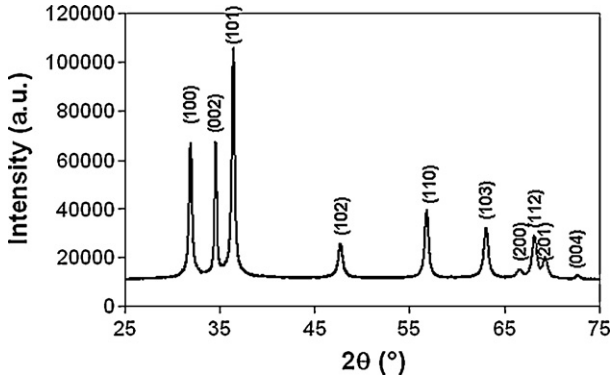

Fig. 1. XRD pattern of $ZnO_{[0.11]}$ synthesized at pH = 5.6 without an additive. Similar patterns were recorded for all samples, with and without additives.

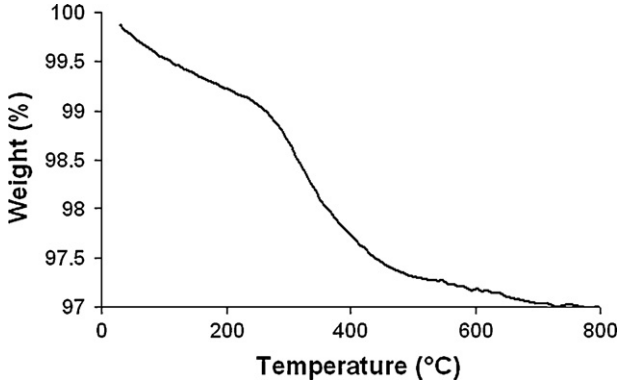

Fig. 2. TG curve obtained for sample $ZnO_{[0.11]}$ synthesized at pH = 5.6 without an additive (heating rate 10 °C min^{-1} in flowing air 30 mL min^{-1}).

Table 3
Weight loss measured at 500 and 800 °C from TG curves of ZnO powders.

Sample	Weight loss at 500 °C [%]	Weight loss at 800 °C [%]
$ZnO_{[0.11]}$	2.7	2.9
$ZnO_{[SDS]}$	6.4	6.5
$ZnO_{[fru]}$	4.6	4.8
$ZnO_{[HPMC]}$	4.6	4.7
$ZnO_{[pvp8000]}$	3.0	3.4
$ZnO_{[PVP40,000]}$	3.1	3.5
$ZnO_{[Disp]}$	6.2	6.3
$ZnO_{[PAA]}$	14.4	14.5
$ZnO_{[PAA-1.5]}$	0.7	1.1

Only a small increase of the total weight loss was observed with Fructose, HPMC, PVP 8000, and PVP 40,000, indicating very little adsorption. A higher weight loss was observed with SDS and Dispex A40, around 6.3–6.5 wt.%, corresponding to around 3 wt.% of adsorbed polymer. The highest affinity was observed for the low molecular weight PAA with 11.7 wt.% of adsorbed polymer. Finally the material synthesized in basic conditions ($ZnO_{[PAA-1.5]}$) showed a lower weight loss compared to $ZnO_{[0.11]}$, despite the presence of PAA in the reaction mixture, consistent with the low S_{BET}.

3.4. Microscopy (SEM)

The morphologies of the synthesized powders can be observed in the SEM micrographs presented in Fig. 3. $ZnO_{[0.11]}$ synthesized at pH = 5.6 without an additive was composed of roundish particles of 200–300 nm, made of aggregated primary particles of smaller sizes (Fig. 3(a)). This powder presented a good homogeneity in size and morphology. Similar powder characteristics were obtained with the additives Fructose, HPMC, PVP 8000 and PVP 40,000 (Fig. 3(c)–(f)). The particle size was reduced by the addition of SDS (Fig. 3(b)), Dispex A40 (Fig. 3(g)) and PAA 2000 (Fig. 3(h)). They led to small and homogeneous roundish particles around 100 nm.

Morphologies obtained with PAA 2000 in basic conditions were very different (Fig. 3(i) and (j)). These particles presented flower-like morphologies with an aspect ratio increasing as the amount of NaOH increased, from 2 in $ZnO_{[PAA-0.22]}$, to 5 in $ZnO_{[PAA-1.5]}$, with the nominal NaOH concentration increasing from 0.22 to 1.5 M, respectively. The growth was oriented along the *c*-axis, leading to nanorods with a hexagonal structure (Fig. 3(j)). This is the "typical" morphology for ZnO precipitates in basic conditions.[9,23,25]

3.5. Particle size distribution (CPS)

Particle size distributions (PSD) for all powders are presented in Fig. 4. The three characteristic sizes (d_{v10}, d_{v50}, d_{v90}) of the PSD are given in Table 4. The span of the PSD is calculated from Eq. (4), and gives an indication of the width of the PSD:

$$\text{span} = \frac{d_{v90} - d_{v10}}{d_{v50}} \quad (4)$$

A d_{v50} of 287 nm (agglomeration factor ($F_{agg} = 2.6$)) was measured for $ZnO_{[0.11]}$ obtained at low pH without an additive. The addition of Fructose, HPMC, PVP 8000 and PVP 40,000 led to a small increase in d_{v50}, but remained below 500 nm. SDS, Dispex A40 and PAA 2000 addition led to a significant decrease of d_{v50}, to 89, 135 and 105 nm, respectively. These powders also presented a lower agglomeration factor (Table 4). Increasing the pH led to a significant increase of d_{v50} to 800 nm, but the morphology was so far from the spherical optical model used in the detection method, that this figure is only qualitative. A striking result is that whatever the conditions the span was very small (below 1), which indicates the materials were very homogeneous in size in all cases. Also the agglomeration factor was very small (<3) for all the samples. A wide range of sizes, around one order of magnitude, is covered by these 10 powders.

4. Discussion

4.1. Thermodynamic considerations

The main species in solution for the reaction (Eq. (1)) were calculated using the thermodynamic software StreamAnalyser from Oli Systems.[b] This predictive thermodynamic model is widely used in the chemical and engineering industries, in oil and gas, as well as in research institutes. Oli model is based upon published experimental data. A large thermodynamic databank is available, covering most of the periodic table of elements. We consider $[Zn^{2+}] = 0.10$ M with increasing concentrations of NaOH at 90 °C. The results of the calculation are presented in Fig. 5(a), showing the main species as a function of the pH of the reaction medium in Fig. 5(b).

Below NaOH = 0.10 M, Zn^{2+} is the main dissolved species, in equilibrium with ZnO as the precipitated phase. For a concentration of NaOH = 0.11 M, the model predicts the pH of the reaction mixture to be 5.3 (Fig. 5(b)), which is close to the experimental value of 5.6 at this concentration (Table 1). The main solid phase is ZnO in these conditions. By increasing the amount of NaOH, $Zn(OH)_4^{2-}$ becomes the main dissolved species in equilibrium with ZnO. For NaOH concentrations of 0.22 and 1.5 M, the model predicts a pH of 10.6 and 12.3, respectively, which are close to the measured values of 11.2 and 12.5 for $ZnO_{[PAA-0.22]}$ and $ZnO_{[PAA-1.5]}$. The discrepancies can be attributed to a possible error in solution composition from the starting products. Finally with a concentration of NaOH > 2.3 M and a pH > 12.5, the model no longer predicts the precipitation of ZnO but a predominance of $Zn(OH)_4^{2-}$.

4.2. Characteristics of the powder obtained at pH 5.6 without additive

The synthesis conducted at pH 5.6 led to the instantaneous precipitation of regular submicronic roundish particles of pure and well crystallised ZnO ($ZnO_{[0.11]}$). The size of the primary particles calculated with the BET method (112 nm) was higher

[b] http://www.olisystems.com/.

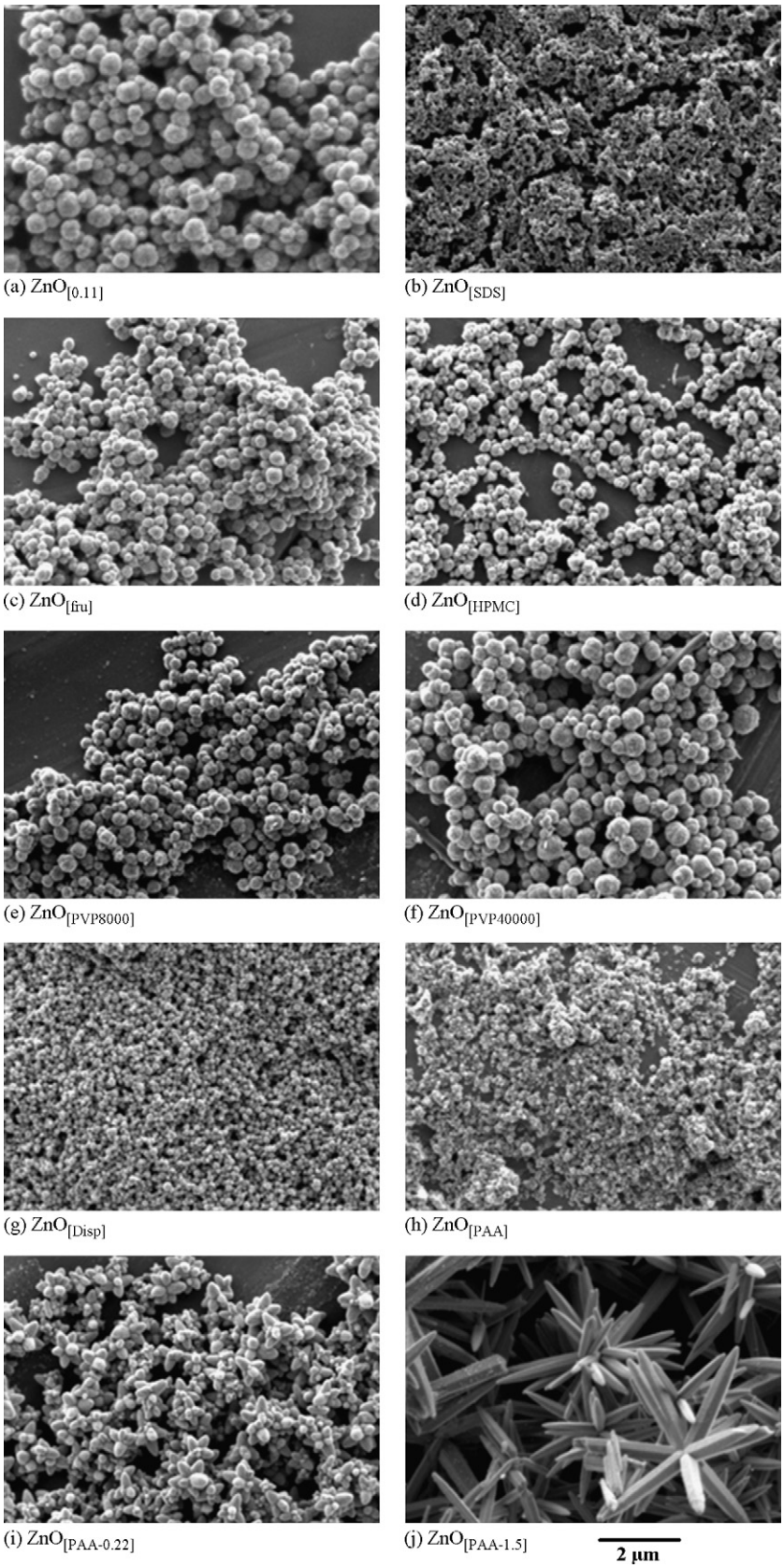

Fig. 3. SEM micrographs of ZnO powders from different synthesis conditions (magnification 10,000×): (a) pH = 5.6 without additive, (b–h) pH = 5.6 with 0.05 wt.% of different additives, (i) pH = 11.2 with 0.05 wt.% PAA 2000, and (j) pH = 12.5 with 0.05 wt.% PAA 2000.

Table 4
Particle size distribution of ZnO powders. For $ZnO_{[PAA]}$, $ZnO_{[Disp]}$ and $ZnO_{[SDS]}$, d_{BET} is calculated using the S_{BET} measured after a heat-treatment of 10 min at 500 °C for the calculation of F_{agg}.

Sample	d_{v10} [nm]	d_{v50} [nm]	d_{v90} [nm]	Span, $(d_{v90} - d_{v10})/d_{v50}$	F_{agg}, d_{v50}/d_{BET}
$ZnO_{[0.11]}$	162	287	365	0.71	2.6
$ZnO_{[SDS]}$	60	89	134	0.83	2.2
$ZnO_{[fru]}$	232	357	476	0.68	2.6
$ZnO_{[HPMC]}$	147	300	431	0.95	2.8
$ZnO_{[pvp8000]}$	259	401	520	0.65	2.4
$ZnO_{[PVP40,000]}$	258	431	580	0.75	2.9
$ZnO_{[Disp]}$	82	135	195	0.84	1.6
$ZnO_{[PAA]}$	68	105	148	0.76	1.4
$ZnO_{[PAA-0.22]}$	364	646	855	0.76	
$ZnO_{[PAA-1.5]}$	560	800	1100	0.68	2.2

than the crystallite size calculated from the Scherrer equation along [1 0 0] (27 nm), which indicates particles are polycrystalline. The d_{v50} was 287 nm, the F_{agg} 2.6, with a narrow span of 0.71. This material already presents very good features which should lead to a ceramic of high quality after sintering.

Most work in the literature has been made in basic conditions, leading to a preferential growth along the *c*-axis to form 1D morphologies (nanorods, star-like or flower-like shapes).[9,23,25] The growth mechanism of such structures has been explained by an electrostatically driven growth mechanism. At basic pH the $Zn(OH)_4^{2-}$ complexes are the dominant species in solution (see Fig. 5, and Eqs. (5) and (6)), and are assumed to adsorb preferentially on the (0 0 0 1) positive surface of ZnO, leading to a preferential growth in this direction

$$Zn^{2+} + 4HO^- \rightarrow Zn(OH)_4^{2-} \quad (5)$$

$$Zn(OH)_4^{2-} \rightarrow ZnO + 2HO^- + H_2O \quad (6)$$

In our study the formation of regular roundish particles can be attributed to the lower pH conditions (pH = 5.6). Zn^{2+} is then the main dissolved species (Fig. 5). There is no longer an electrostatic driving force for preferential growth.

The good homogeneity in size and shape was attributed to a good control of the precipitation route. The very fast mixing of the reactants (50–100 ms[19]) allows a high nucleation rate, leading to the formation of particles in the nanometre range. The injection device used (Y mixer) allows a homogeneous mixing, and consequently a homogeneous crystal growth, leading to a narrow size distribution.

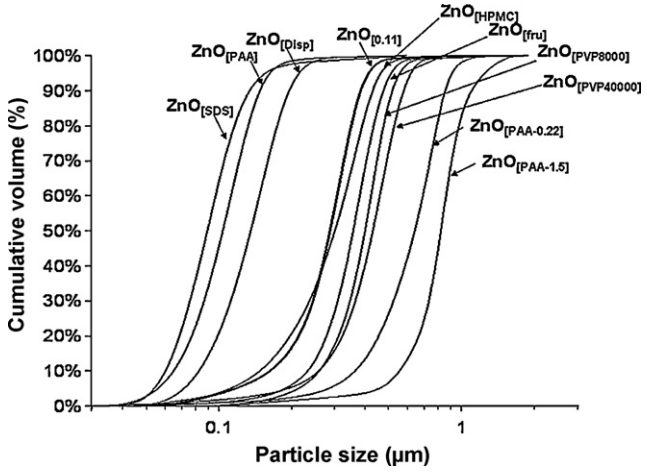

Fig. 4. Particle size distributions of ZnO powders measured by centrifugal sedimentation (CPS).

4.3. Effect of additives at pH 5.6

The effect of different additives on the precipitated zinc oxide has been studied at low pH (pH = 5.6). Fructose, HPMC, PVP

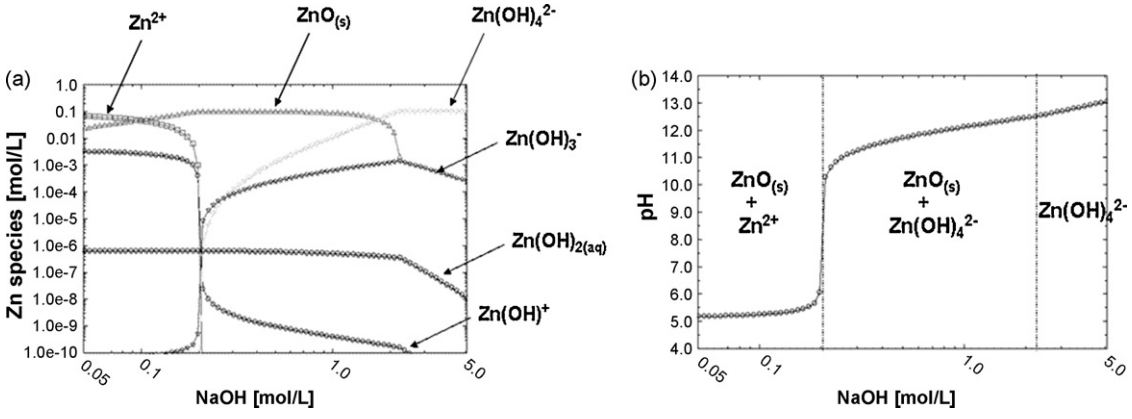

Fig. 5. (a) Thermodynamic data showing the evolution of the concentration of Zn aqueous species in the reaction mixture at 90 °C depending on NaOH concentration with $[Zn^{2+}] = 0.10$ M. (b) Theoretical evolution of the pH in the same conditions, with dominant species.

8000 and PVP 40,000 had no significant effect on morphology or crystallite size. Weight loss measured by TGA showed that only a small amount of these polymers are adsorbed at the surface of the material (<9 mg/g of powder). They led to a small increase in the d_{v50} up to 300–400 nm. For all these materials, the narrow PSD was conserved (span < 1), and the F_{agg} remained low between 2.2 and 2.8. Fructose and HPMC belong to the carbohydrates, and are widely used to stabilize drug suspensions by adsorption via hydrogen bonding.[26,27] Polyvinylpyrrolidone was chosen as a non-ionic polyelectrolyte. It is used as a stabilizer to prevent agglomeration in coating latex or silica colloids with metal,[28] and can also stabilise ceramic, metallic and drug suspensions by forming hydrogen bonds.[26,29,30] The precipitation of zinc oxide was not affected by such polymers, because there is little interaction with ZnO surface.

In contrast, SDS, Dispex A40 and PAA 2000 led to a decrease of the d_{v50} which was also qualitatively observed in SEM micrographs. They also presented a lower F_{agg} around 1.5 and conserved a very narrow PSD (span around 0.8) whereas the S_{BET}s increased significantly. It has been recently shown by AFM analysis that carboxylic groups (COO^-) have a preference for adhesion on zinc-terminated ZnO faces, such as the (0 0 0 1) surface.[31] At the pH of the reaction (pH = 5.6), PAA is partly dissociated (~35%).[32] The carboxylic groups may preferentially adsorb on the (0 0 0 1) face to inhibit the crystal growth in the direction of the *c*-axis, which is the natural preferential growth direction. This explains that the crystal growth, as well as the agglomeration, is limited in the presence of PAA 2000 and Dispex A40. The difference between these two polymers is the molecular weight (M_w = 2000 for PAA 2000, M_w = 10,000 for Dispex A40). It seems that PAA of smaller size has a greater effect on the crystal growth inhibition. This has also been observed for the crystal growth of gypsum where M_w 2000 seems to be an optimum molecular weight.[33] This may be due to a more efficient adsorption and higher surface coverage of the ZnO particles.

SDS is an anionic surfactant with sulfate head groups (SO_4^-), such groups could act in the same way as carboxylic groups. The small length of its molecular chain compared to PAA 2000 and Dispex A40 could allow it to adsorb quicker and in higher amounts, leading to smaller particle sizes as shown by d_{v50}, and d_{BET} after heat treatment.

The ZnO powders produced using the anionic additives show high quality and should prove to be excellent powders for processing and sintering of zinc oxide ceramics. The next step to fulfil this promise is to produce larger quantities of powders (~100 g) using the SFTR technology which allows scale up of such batch methods without loss of powder quality.[34]

4.4. Effect of PAA in basic conditions

As PAA 2000 had a significant influence on the ZnO nanoparticles precipitation, two more syntheses were made in basic conditions (pH = 11.2 and 12.5), by adding higher amounts of NaOH. In these conditions PAA is fully dissociated, thus we expected a higher growth limitation by a higher adsorption rate at the surface of the particles. Nevertheless the results showed that in basic conditions the particles presented a completely different morphology: a "flower-like" morphology with particle sizes in the micrometre range (Fig. 3(i) and (j)). The crystallite size of the material synthesized at pH 12.5 was higher than for the other syntheses, but remained in the nanometre range (41 nm along [1 0 0] and [0 0 2]). The S_{BET} was smaller (2.9 $m^2\,g^{-1}$) and corresponding d_{BET} and d_{v50} were not reliable, as the morphologies were too far from the spherical assumptions made in these two models.[35] The weight loss measured by TGA was low (1.1%) indicating that little or no polymer was adsorbed at the surface.

In these basic conditions $Zn(OH)_4^{2-}$ is the major dissolved specie (see Fig. 5, and Eq. (5) and (6)). Considering the previous observations, a preferential adsorption of $Zn(OH)_4^{2-}$ on the (0 0 0 1) positive surface of the crystal occurs, leading to a preferential crystal growth along the c axis to form the "flower" shape, and not to the expected inhibition through PAA adsorption on the same surface. This can probably be attributed to kinetic effect where the PAA is too "slow" compared to the molecular $Zn(OH)_4^{2-}$ species. With a lower initial concentration of NaOH, the crystal growth was lower, leading to a lower aspect ratio in $ZnO_{[PAA\text{-}0.22]}$ than in $ZnO_{[PAA\text{-}1.5]}$, as observed in SEM pictures.

5. Conclusions

Pure and crystalline zinc oxide was successfully synthesized using mild hydrothermal conditions (90 °C) with 30 min of ageing. The final powder presents nanometric particles with very narrow size distributions (span < 1). The size and morphology of the precipitated ZnO can be tuned with the addition of polymers, or by modifying the pH. The anionic additives PAA 2000, Dispex A40 and SDS reduce the final particle size and degree of agglomeration by an assumed preferential adsorption on the (0 0 0 1) positive surface, leading to non-agglomerated nanoparticles (around 100 nm) with a narrow size distribution. These features make these materials very interesting for further applications in electronic devices, and should allow a high density after sintering. By conducting the synthesis in basic conditions the morphology was modified towards a flower-like shape, with an aspect ratio of the primary particles increasing with the pH. This characteristic could be exploited to form nanorods in a fast and easy way at high production rates.

References

1. Clarke, D. R., Varistor ceramics. *J. Am. Ceram. Soc.*, 1999, **82**(3), 485–502.
2. Strachowski, T., Grzanka, E., Lojkowski, W., Presz, A., Godlewski, M., Yatsunenko, S. *et al.*, Morphology and luminescence properties of zinc oxide nanopowders doped with aluminum ions obtained by hydrothermal and vapor condensation methods. *J. Appl. Phys.*, 2007, **102**(7), 073513–73519.
3. Wang, Z. L., Nanostructures of zinc oxide. *Mater. Today*, 2004, **7**(6), 26–33.
4. Milošević, O., Uskoković, D., Karanović, L. J., Tomašević-Čanović, M. and Trontelj, M., Synthesis of ZnO-based varistor precursor powders by means of the reaction spray process. *J. Mater. Sci.*, 1993, **28**(19), 5211–5217.
5. Htay, M. T., Hashimoto, Y. and Ito, K., Growth of ZnO submicron single-crystalline platelets, wires, and rods by ultrasonic spray pyrolysis. *Jpn. J. Appl. Phys.*, 2007, **46**, 440–448.

6. Taubert, A., Palms, D., Weiss, O., Piccini, M. and Batchelder, D., Polymer-assisted control of particle morphology and particle size of zinc oxide precipitated from aqueous solution. *Chem. Mater.*, 2002, **14**(6), 2594–2601.
7. Oliveira, A., Hochepied, J., Grillon, F. and Berger, M., Controlled precipitation of zinc oxide particles at room temperature. *Chem. Mater.*, 2003, **15**(16), 3202–3207.
8. Zhang, H., Feng, J., Wang, J. and Zhang, M., Preparation of ZnO nanorods through wet chemical method. *Mater. Lett.*, 2007, **61**(30), 5202–5205.
9. Zhong, Q. and Matijevic, E., Preparation of uniform zinc oxide colloids by controlled double-jet precipitation. *J. Mater. Chem.*, 1996, **6**(3), 443–447.
10. Piticescu, R. R., Piticescu, R. M. and Monty, C. J., Synthesis of Al-doped ZnO nanomaterials with controlled luminescence. *J. Eur. Ceram. Soc.*, 2006, **26**(14), 2979–2983.
11. Hu, H., Huang, X., Deng, C., Chen, X. and Qian, Y., Hydrothermal synthesis of ZnO nanowires and nanobelts on a large scale. *Mater. Chem. Phys.*, 2007, **106**(1), 58–62.
12. Dem'yanets, L., Li, L. and Uvarova, T., Hydrothermal synthesis and cathodoluminescence of ZnO crystalline powders and coatings. *J. Cryst. Growth*, 2006, **287**(1), 23–27.
13. Shen, L., Bao, N., Yanagisawa, K., Gupta, A., Domen, K. and Grimes, C. A., Controlled synthesis and assembly of nanostructured ZnO architectures by a solvothermal soft chemistry process. *Cryst. Growth Des.*, 2007, **7**(12), 2742–2748.
14. Ahmad, T., Vaidya, S., Sarkar, N., Ghosh, S. and Ganguli, A. K., Zinc oxalate nanorods: a convenient precursor to uniform nanoparticles of ZnO. *Nanotechnology*, 2006, **17**(5), 1236–1240.
15. Hung, C. and Whang, W., A novel low-temperature growth and characterization of single crystal ZnO nanorods. *Mater. Chem. Phys.*, 2003, **82**(3), 705–710.
16. Mezy, A., Gerardin, C., Tichit, D., Ravot, D., Suwanboon, S. and Tedenac, J., Morphology control of ZnO nanostructures. *J. Ceram. Soc. Jpn.*, 2008, **116**(1351), 369–373.
17. Jongen, N., Donnet, M., Bowen, P., Lemaitre, J., Hofmann, H., Schenk, R. *et al.*, Development of a continuous segmented flow tubular reactor and the scale-out concept—in search of perfect powders. *Chem. Eng. Technol.*, 2003, **26**(3), 303–305.
18. Jongen, N., Bowen, P., Lemaitre, J., Valmalette, J. and Hofmann, H., Precipitation of self-organized copper oxalate polycrystalline particles in the presence of hydroxypropylmethylcellulose (HPMC): control of morphology. *J. Colloid Interface Sci.*, 2000, **226**(2), 189–198.
19. Donnet, M., Bowen, P., Jongen, N., Lemaitre, J. and Hofmann, H., Use of seeds to control precipitation of calcium carbonate and determination of seed nature. *Langmuir*, 2005, **21**(1), 100–108.
20. Aschauer, U., Jones, F., Richmond, W., Bowen, P., Rohl, A., Parkinson, G. *et al.*, Growth modification of hematite by phosphonate additives. *J. Cryst. Growth*, 2008, **310**(3), 688–698.
21. Zhang, J., Liu, H., Wang, Z., Ming, N., Li, Z. and Biris, A., Polyvinylpyrrolidone-directed crystallization of ZnO with tunable morphology and bandgap. *Adv. Funct. Mater.*, 2007, **17**(18), 3897–3905.
22. Shang, T., Sun, J., Zhou, Q. and Guan, M., Controlled synthesis of various morphologies of nanostructured zinc oxide: flower, nanoplate, and urchin. *Cryst. Res. Technol.*, 2007, **42**(10), 1002–1006.
23. Zhu, H., Yang, D. and Zhang, H., A simple and novel low-temperature hydrothermal synthesis of ZnO nanorods. *Inorg. Mater.*, 2006, **42**(11), 1210–1214.
24. Li, P., Wei, Y., Liu, H. and Wang, X., Growth of well-defined ZnO microparticles with additives from aqueous solution. *J. Solid State Chem.*, 2005, **178**(3), 855–860.
25. Ge, J., Tang, B., Zhuo, L. and Shi, Z., A rapid hydrothermal route to sisal-like 3D ZnO nanostructures via the assembly of CTA+ and $Zn(OH)_4^{2-}$: growth mechanism and photoluminescence properties. *Nanotechnology*, 2006, **17**(5), 1316–1322.
26. Raghavan, S. L., Trividic, A., Davis, A. F. and Hadgraft, J., Crystallization of hydrocortisone acetate: influence of polymers. *Int. J. Pharm.*, 2001, **212**(2), 213–221.
27. Raghavan, S. L., Schuessel, K., Davis, A. and Hadgraft, J., Formation and stabilisation of triclosan colloidal suspensions using supersaturated systems. *Int. J. Pharm.*, 2003, **261**(1–2), 153–158.
28. Zhang, J., Liu, J., Wang, S., Zhan, P., Wang, Z. and Ming, N., Facile methods to coat polystyrene and silica colloids with metal. *Adv. Funct. Mater.*, 2004, **14**(11), 1089–1096.
29. Sekikawa, H., Nakano, M. and Arita, T., Inhibitory effect of polyvinylpyrrolidone on the crystallization of drugs. *Chem. Pharm. Bull.*, 1978, **26**(1), 118–126.
30. Tantishaiyakul, V., Kaewnopparat, N. and Ingkatawornwong, S., Properties of solid dispersions of piroxicam in polyvinylpyrrolidone. *Int. J. Pharm.*, 1999, **181**(2), 143–151.
31. Golovko, D., Munoz-Espi, R. and Wegner, G., Interaction between poly(styrene–acrylic acid) latex nanoparticles and zinc oxide surfaces. *Langmuir*, 2007, **23**(7), 3566–3569.
32. Hackley, V. A., Colloidal processing of silicon nitride with poly(acrylic acid): I. Adsorption and electrostatic interactions. *J. Am. Ceram. Soc.*, 1997, **80**(9), 2315–2325.
33. Oner, M., Dogan, O. and Oner, G., The influence of polyelectrolytes architecture on calcium sulfate dihydrate growth retardation. *J. Cryst. Growth*, 1998, **186**(3), 427–437.
34. Bowen, P., Testino, A., Legagneur, V., Donnet, M., Hofmann, H. and Cobut, N., Precipitation of nanostructured & ultrafine powders: process intensification using the segmented flow tubular reactor—still in search of the perfect powder?". In *Proceedings of Fifth World Congress on Particle Technology (WCPT5)*, 2006.
35. Bowen, P., Particle size distribution measurement from millimeters to nanometers and from rods to platelets. *J. Disper. Sci. Technol.*, 2002, **23**(5), 631.